Journal of Solid State Chemistry 182 (2009) 1297–1303

Contents lists available at ScienceDirect

Journal of Solid State Chemistry

journal homepage: www.elsevier.com/locate/jssc

Charge density matching in templated molybdates

Hernan Sanchez Casalongue [a], Sarah J. Choyke [a], Amy Narducci Sarjeant [b], Joshua Schrier [a], Alexander J. Norquist [a,*]

[a] Department of Chemistry, Haverford College, Haverford, PA 19041, USA
[b] Department of Chemistry, Johns Hopkins University, Baltimore, MD 21218, USA

ARTICLE INFO

Article history:
Received 18 December 2008
Received in revised form
24 February 2009
Accepted 27 February 2009
Available online 6 March 2009

Keywords:
Charge density matching
Polyoxomolybdate
Hydrothermal

ABSTRACT

The role of charge density matching in the formation of templated molybdates under mild hydrothermal conditions was investigated through the use of a series of structurally related amines: piperazine, 1,4-dimethylpiperazine, 2,5-dimethylpiperazine and 2,6-dimethylpiperazine. A series of reactions was conducted in which the relative mole fractions of each component were fixed at 2.5 MoO_3:1 amine:330 H_2O:2 H_2SO_4 in order to isolate the effects of the amine, the only variation between reactions was the structure of the amine. Four distinct polyoxomolybdates anions were observed, ranging from zero-dimensional β-$[Mo_8O_{26}]^{4-}$ molecular anions to $[Mo_3O_{10}]_n^{2n-}$ and $[Mo_8O_{26}]_n^{4n-}$ chains and $[Mo_5O_{16}]_n^{2n-}$ layers. The primary influence over the structure of the molybdate anion is charge density matching with the protonated amine, which was quantified through surface area approximations based upon both calculated molecular surfaces and polyhedral representations of each anion. Secondary influences include amine symmetry and hydrogen-bonding preferences. The synthesis and characterization of two new compounds are reported. Crystal data: $[C_6H_{16}N_2][Mo_3O_{10}]\cdot H_2O$ (**1**), triclinic, *P*-1 (no. 2), $a = 8.0973(7)$ Å, $b = 8.8819(9)$ Å, $c = 11.5969(11)$ Å, $\alpha = 71.362(9)^\circ$, $\beta = 82.586(8)^\circ$, $\gamma = 74.213(8)^\circ$, $Z = 2$, $R/R_w = 0.0262/0.0564$, and $[C_6H_{16}N_2]_2[Mo_8O_{26}]$ (**2**), monoclinic, $P2_1/n$ (no. 14), $a = 7.9987(11)$ Å, $b = 12.5324(19)$ Å, $c = 16.003(3)$ Å, $\beta = 97.393(14)^\circ$, $Z = 2$, $R/R_w = 0.0189/0.0454$.

1. Introduction

The synthesis of new materials under hydrothermal conditions using amine structure directing agents has been employed to produce a host of new materials over the past decades [1–4]. Despite the versatility of hydrothermal conditions and the maturity of this chemistry, it is not currently possible to design a reaction product and synthesize it cleanly after choosing a set of reactants and reaction conditions. While a wide range of trends have been observed, leading to the formation of several generalizations, true prediction remains largely elusive.

A number of reaction mechanisms have been postulated for the formation of several families of microporous solids [4–7], including those predicted using modeling [8,9]. It has been proposed by Ferey [4,5] that organic amines provide the driving force for the formation of organically templated inorganic materials. He postulated that charge density matching between the amine and secondary building unit (SBU) results in neutral ammonium–SBU pairs, which allow for precipitation. The charge densities of the amines are generally fixed by pH, while structural modulations in the inorganic components allow for the formation of neutral pairs.

The determination of accurate charge densities is dependent upon the availability of surface area data. Suitable definitions of molecular, contact and reentrant surface areas in macromolecules were developed by Richards in 1977, for the study of protein structure and function [10]. This method works well in such systems because spherical probe approximations are valid for water. However, the non-spherical nature of many organic amines must be addressed.

The effects of charge density matching have been demonstrated in several systems using different methods. These include the work of Stucky et al. on transformations between lamellar and hexagonal silicate mesophases [11–13] and oxovanadium phosphate mesostructure chemistry by Marcos and Amorós et al. [14] More recently, Maggard et al. [15], Krivovichev et al. [16] and Burns et al. [17] have discussed methods for calculating charge densities in polyoxovanadate/metal–ligand compounds and uranyl selenates.

Our approach to study the role of charge density matching in the formation of new templated materials involves both the use of a series of structurally related amines that exhibit different charge densities and the development of a method for the approximation of the surface area of inorganic structures of varying dimensionality. Piperazine (pip), 1,4-dimethylpiperazine

* Corresponding author.
E-mail address: anorquis@haverford.edu (A.J. Norquist).

0022-4596/$ - see front matter © 2009 Elsevier Inc. All rights reserved.
doi:10.1016/j.jssc.2009.02.032

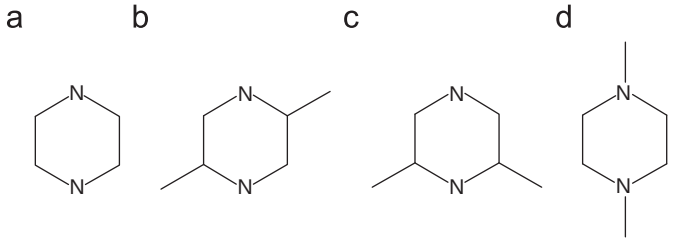

Fig. 1. Structures of the four amines used in this study: (a) piperazine, (b) 2,5-dimethylpiperazine, (c) 2,6-dimethylpiperazine and (d) 1,4-dimethylpiperazine.

(1,4-dmpip), 2,5-dimethylpiperazine (2,5-dmpip) and 2,6-dimethylpiperazine (2,6-dmpip) were used in four reactions in which the only difference in gel composition was the identity of the amine. See Fig. 1. This allows for the direct observation of the effects of amine structure on the resulting solid. The synthesis and characterization of two new compounds are reported: $[C_6H_{16}N_2][Mo_3O_{10}]\cdot H_2O$ (**1**) and $[C_6H_{16}N_2]_2[Mo_8O_{26}]$ (**2**).

2. Experimental

Materials: MoO_3 (99.5%), piperazine (99%), 1,4-dimethylpiperazine (98%), 2,5-dimethylpiperazine (98%), 2,6-dimethylpiperazine (97%), sulfuric acid (95–98%), hydrochloric acid (37%) and KOH (85%) were purchased from Aldrich and used as received. Deionized water was used in these syntheses.

Synthesis: All reactions were conducted in 23 mL poly(fluoroethylene-propylene) lined pressure vessels and balanced to a pH of 5 by addition of hydrochloric acid and aqueous 30% KOH. Reactions were heated to 150 °C over 30 min and allowed to soak for 24 h. The reactions were then cooled to room temperature at a rate of 6 °C h^{-1}. Autoclaves were opened in air, and products were recovered through filtration. Powder X-ray diffraction patterns of each bulk sample match the pattern generated from the respective single-crystal X-ray structure data.

$[C_6H_{18}N_2]_2[Mo_8O_{26}]$ (**1**) was synthesized through the reaction of 0.5734 g (2.56×10^{-3} mol) of MoO_3, 0.1169 g (1.03×10^{-3} mol) of 2,6-dmpip, 0.2084 g (1.99×10^{-3} mol) of H_2SO_4, 6.0172 g (3.34×10^{-1} mol) of deionized water. Colorless plates. Elemental microanalysis for **1** obsd (calc.): C 12.37(12.36); H 3.09(2.78); N 4.81(4.79). IR data: N–H 1469, 1622 cm^{-1}, C–H 2969 cm^{-1}, Mo═O 939 cm^{-1}.

$[C_6H_{18}N_2]_2[Mo_8O_{26}]$ (**2**) was synthesized through the reaction of 0.5757 g (2.57×10^{-3} mol) of MoO_3, 0.1162 g (1.02×10^{-3} mol) of 1,4-dmpip, 0.1991 g (2.03×10^{-3} mol) of H_2SO_4, 6.0194 g (3.34×10^{-1} mol) of deionized water. Colorless blocks. Elemental microanalysis for **2** obsd (calc.): C 7.10(10.1); H 1.36(2.26); N 2.76(3.96). IR data: N–H 1458, 1577 cm^{-1}, C–H 3150 cm^{-1}, Mo═O 941 cm^{-1}.

Single crystal X-ray diffraction: Data were collected using an Oxford Diffraction, Xcalibur3 CCD diffractometer with an enhanced Mo*K*α radiation ($\lambda = 0.71073$ Å). A single crystal was mounted on a glass fiber using *N*-paratone oil and cooled *in-situ* to 110(2) K for data collection. Frames were collected, indexed, processed and the files scaled using CrysAlis RED [18]. The heavy atom positions were determined using SIR92 [19]. All other non-hydrogen sites were located from Fourier difference maps. All non-hydrogen sites were refined using anisotropic thermal parameters using full matrix least squares procedures on F_0^2 with $I>3\sigma(I)$. Hydrogen atoms were placed in geometrically idealized positions. All calculations were performed using Crystals [20]. Relevant crystallographic data are listed in Table 1.

Powder X-ray diffraction: Powder diffraction patterns were recorded on a GBC-Difftech MMA powder diffractometer. Samples were mounted on aluminum plates. Calculated powder patterns were generated from single crystal data using ATOMS *v.* 6.0 [21].

Table 1
Crystallographic data for compounds **1** and **2**.

Compound	$[C_6H_{16}N_2][Mo_3O_{10}]\cdots H_2O$ (**1**)	$[C_6H_{16}N_2]_2[Mo_8O_{26}]$ (**2**)
Formula	$C_6H_{18}Mo_3N_2O_{11}$	$C_{12}H_{32}Mo_8N_4O_{26}$
fw	582.04	1415.92
Space-group	*P*-1 (no. 2)	$P2_1/n$ (no. 14)
a (Å)	8.0973(7)	7.9987(11)
b (Å)	8.8819(9)	12.5324(19)
c (Å)	11.5969(11)	16.003(3)
α (deg)	71.362(9)	90
β (deg)	82.586(8)	97.393(14)
γ (deg)	74.213(8)	90
V (Å^3)	763.10(13)	1590.9(5)
Z	2	2
ρ_{calc} (g cm^{-3})	2.533	2.956
λ (Å)	0.71073	0.71073
T (K)	110(2)	110(2)
μ (mm^{-1})	2.484	3.153
R_1[a]	0.0262	0.0189
wR_2[b]	0.0564	0.0454

[a] $R_1 = \Sigma||F_0|-|F_c||/\Sigma|F_0|$.
[b] $wR_2 = [\Sigma w(F_0^2-F_c^2)^2/[\Sigma w(F_0^2)^2]^{1/2}$.

Infrared spectroscopy: Infrared measurements were obtained using a Perkin Elmer FT-IR Spectrum 1000 spectrophotometer. Samples were diluted with spectroscopic grade KBr and pressed into a pellet. Scans were run over the range of 400–4000 cm^{-1}.

Surface area calculations: Surface areas for the polyoxomolybdate components in **1**, **2**, $[C_6H_{16}N_2]_2[Mo_8O_{26}]$ [22] and $[C_4H_{12}N_2][Mo_5O_{16}]$ [23] were calculated using two different methods. First, the molecular surface, defined by Richards as the composite of the van der Waals contact surface and the reentrant surface of the molecule [10] was calculated using the DMS program [24]. A probe radius of 1.5 Å was used to mimic the amine–oxygen hydrogen bonding distance, and van der Waals radii of 1.52 and 2.00 Å for the van der Waals radii of oxygen and molybdenum atoms, respectively. Linear fits, provided in the Supplementary information, were used to remove edge effects from the truncated 1D and 2D structures (Figs. 2–4).

We developed a second method for the determination of surface area by decomposing each anion surface into triangles, with the vertices defined by the outermost oxygen atoms, and then shifted 'outward' from the oxygen atom centers to reflect the 1.52 Å van der Waals radius [25], as illustrated in Figs. 5–8. For the zero-dimensional β-$[Mo_8O_{26}]^{4-}$ molecular anion, this shift was calculated by first determining the geometric center, and then increasing the length of each vector from the center point to the respective vertices by the van der Waals radii. The shift in both one-dimensional chains ($[Mo_3O_{10}]_n^{2n-}$ and $[Mo_8O_{26}]_n^{4n-}$) was calculated by averaging the coordinates in the axes perpendicular to the periodic axis of each chain to determine a center line (parallel to the periodic axis of each anion), and then increasing the length of the vector (in the plane normal to this central line) from the central line to the oxygen atom by the van der Waals radius. No shift was necessary for the surface area calculation of the $[Mo_5O_{16}]_n^{2n-}$ layer because such a shift would consist of moving the position of all the vertices uniformly in the direction normal to the periodic plane of the anion, which does not change the surface area. Multiple models were used for the $[Mo_3O_{10}]_n^{2n-}$ and $[Mo_8O_{26}]_n^{4n-}$ chains and the $[Mo_5O_{16}]_n^{2n-}$ layer. Calculated polyoxomolybdates surface areas and charge densities are listed in Table 2.

Volume calculations: The volume calculations (results shown in the Supplementary data) were performed using Monte Carlo

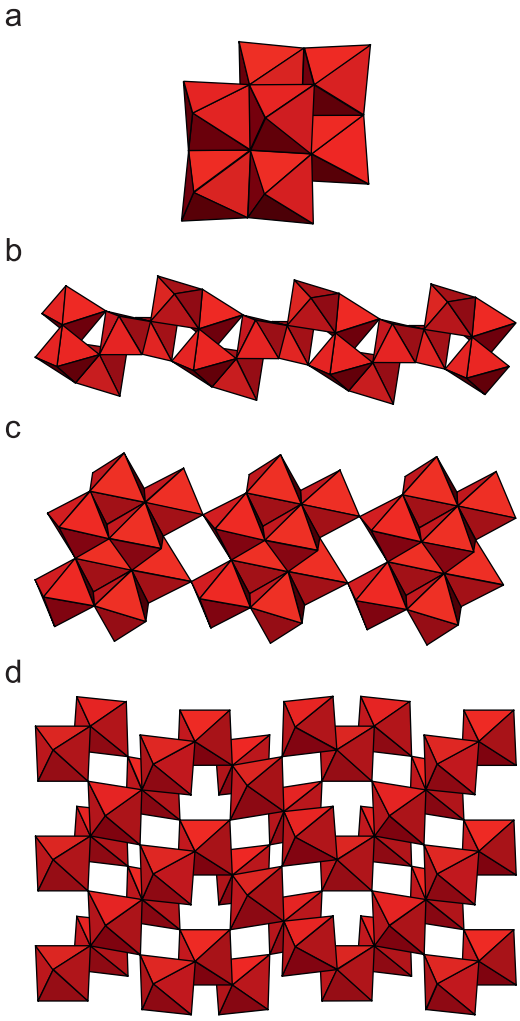

Fig. 2. Polyhedral representations of (a) β-$[Mo_8O_{26}]^{4-}$ molecular ions, (b) $[Mo_3O_{10}]_n^{2n-}$ chains, (c) $[Mo_8O_{26}]_n^{4n-}$ chains and (d) $[Mo_5O_{16}]_n^{2n-}$ layers.

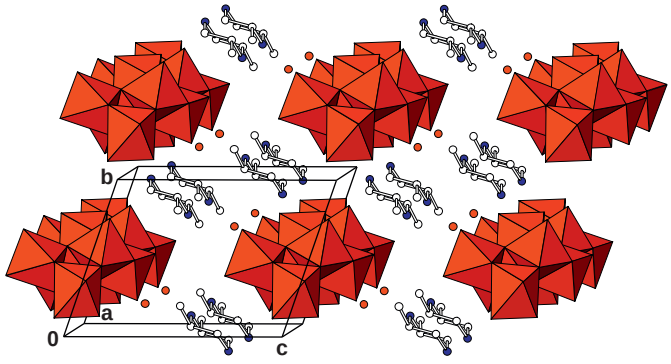

Fig. 3. Three-dimensional packing diagram of $[C_6H_{16}N_2][Mo_3O_{10}]\cdot H_2O$ **(1)**. Red octahedra represent $[MoO_6]$, while white, blue and red circles represent carbon, nitrogen and oxygen, respectively. Hydrogen atoms have been removed for clarity. (For interpretation of the references to color in this figure legend, the reader is referred to the web version of this article.)

integration (converged to $<0.05\%$ relative error in all cases) using tabulated van der Waals radii of Bondi, with the exception of hydrogen for which the van der Waals radius of Rowland and Taylor [26] was used. The anion models were based upon single crystal X-ray diffraction data. A B3LYP/6-31G* geometry optimization of the piperazine molecules was performed using

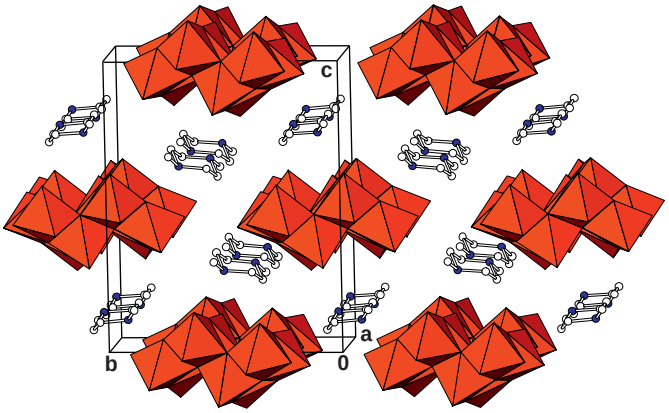

Fig. 4. Three-dimensional packing diagram of $[C_6H_{16}N_2]_2[Mo_8O_{26}]$ **(2)**. Red octahedra represent $[MoO_6]$, while white and blue circles represent carbon and nitrogen, respectively. Hydrogen atoms have been removed for clarity. (For interpretation of the references to color in this figure legend, the reader is referred to the web version of this article.)

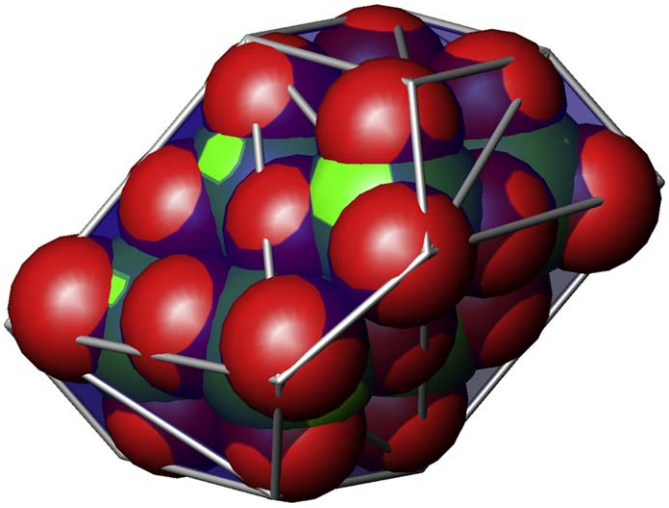

Fig. 5. Space filling representation of the β-$[Mo_8O_{26}]^{4-}$ anion in $[C_6H_{16}N_2]_2[Mo_8O_{26}]$. White lines represent the edges of the triangles used for surface area calculations. Oxygen and molybdenum van der Waals radii of 1.52 and 2.00 Å are used, respectively.

Gaussian03.RevE1 [27] because hydrogen atom locations based upon X-ray diffraction data are unreliable.

3. Results

The inorganic components present in compounds **1**, **2**, $[C_6H_{16}N_2]_2[Mo_8O_{26}]$ [22] and $[C_4H_{12}N_2][Mo_5O_{16}]$ [23] vary in dimensionality and connectivity; however, certain structural features are retained. Each second-order Jahn–Teller [28–31] active molybdenum(VI) center exhibits a distorted octahedral geometry. $Mo–O_{terminal}$ bonds are generally shorter than $Mo–O_{bridging}$ bonds; the observed ranges are 1.698(7)–1.726(4) Å and 1.757(6)–2.396(3) Å, respectively. A much wider spread in $Mo–O_{bridging}$ bonds is observed because the bridging oxides can be bound from anywhere between two and six adjacent molybdenum centers. Four distinct anion connectivities are observed: β-$[Mo_8O_{26}]^{4-}$ molecular anions, $[Mo_3O_{10}]_n^{2n-}$ and $[Mo_8O_{26}]_n^{4n-}$ chains and $[Mo_5O_{16}]_n^{2n-}$ layers. See Fig. 2. The chemistry of polyoxomolybdates has been studied extensively for several

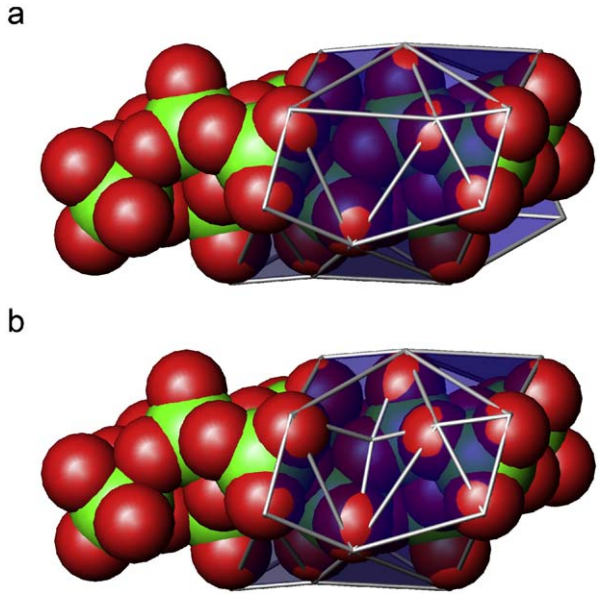

Fig. 6. Space filling representations of the $[Mo_3O_{10}]_n^{2n-}$ chains in **1**. The white lines in (a) and (b) represent the edges of the triangles used for model 1 and model 2 surface area calculations. Oxygen and molybdenum van der Waals radii of 1.52 and 2.00 Å are used, respectively.

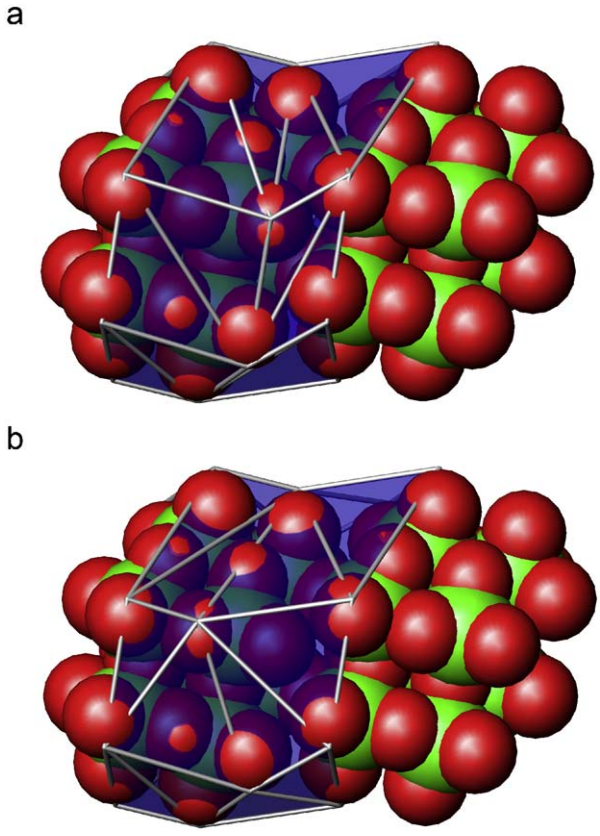

Fig. 7. Space filling representations of the $[Mo_8O_{26}]_n^{4n-}$ chains in **2**. The white lines in (a) and (b) represent the edges of the triangles used for model 1 and model 2 surface area calculations. Oxygen and molybdenum van der Waals radii of 1.52 and 2.00 Å are used, respectively.

decades because of a host of desirable physical properties that compounds containing such anions can exhibit, with reviews of this chemistry appearing elsewhere [32–35].

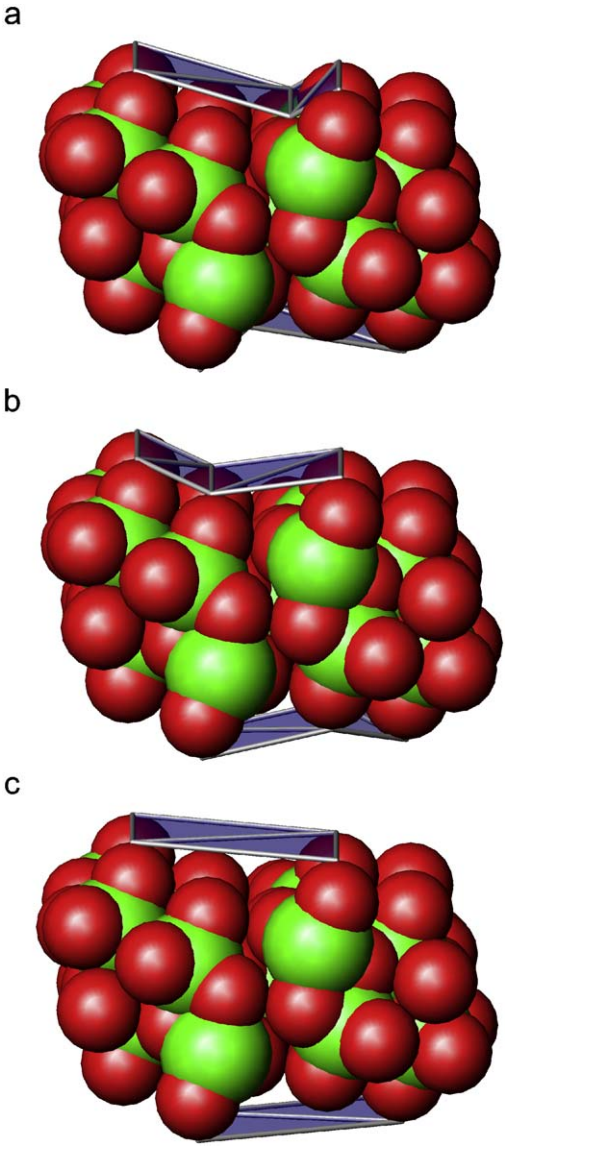

Fig. 8. Space filling representations of the $[Mo_5O_{16}]_n^{2n-}$ layers in $[C_4H_{12}N_2][Mo_5O_{16}]$. The white lines in (a), (b) and (c) represent the edges of the triangles used in model 1, model 2 and model 3 surface area calculations. Oxygen and molybdenum van der Waals radii of 1.52 and 2.00 Å are used, respectively.

β-$[Mo_8O_{26}]^{4-}$: The well-known β-octamolybdate anion [22,36–39] is observed in $[C_6H_{16}N_2]_2[Mo_8O_{26}]$ [22]. These anions are constructed of eight $[MoO_6]$ octahedra that share common edges and vertices with one another to form the anions shown in Fig. 2a.

$[Mo_3O_{10}]_n^{2n-}$: One-dimensional $[Mo_3O_{10}]_n^{2n-}$ chains are present in **1**. See Fig. 2b. The MoO_6 octahedra in $[Mo_3O_{10}]_n^{2n-}$ chains share either two edges and one corner, one edge and one face, or one face, one edge and one corner [40]. The three-dimensional packing of **1** is shown in Fig. 3. This chain connectivity has been previously reported [39–42].

$[Mo_8O_{26}]_n^{4n-}$: One-dimensional $[Mo_8O_{26}]_n^{4n-}$ chains [39,43] constructed from $[Mo_8O_{24}O_{4/2}]_n^{4n-}$ monomers are observed in **2**. These monomers are connected to one another through two shared corners. These chains are shown in Fig. 2c. The three-dimensional packing of **2** is shown in Fig. 4. This chain connectivity has been previously reported [44–47].

$[Mo_5O_{16}]_n^{2n-}$: $[Mo_5O_{16}]_n^{2n-}$ layers, shown in Fig. 2d, are constructed from 'zig-zag' chains of edge shared MoO_6 octahedra,

Table 2
Surface area and charge density results for **1**, **2**, $[C_6H_{16}N_2]_2[Mo_8O_{26}]$ and $[C_4H_{12}N_2][Mo_5O_{16}]$.

Anion	Method	Surface area (Å^2)	Anion charge	Charge density (−/Å^2)
β-$[Mo_8O_{26}]^{4-}$	Geometric decomposition	297	−4	−0.0135
	Molecular surface	329	−4	−0.0122
$[Mo_3O_{10}]_n^{2n-}$	Geometric decomposition			
	Model 1	113	−2	−0.0176
	Model 2	114	−2	−0.0175
	Molecular surface	116	−2	−0.0172
$[Mo_8O_{26}]_n^{4n-}$	Geometric decomposition			
	Model 1	250	−4	−0.0160
	Model 2	248	−4	−0.0161
	Molecular surface	258	−4	−0.0155
$[Mo_5O_{16}]_n^{2n-}$	Geometric decomposition			
	Model 1	87.3	−2	−0.0229
	Model 2	83.2	−2	−0.0240
	Model 3	81.0	−2	−0.0247
	Molecular surface	104	−2	−0.0193

which are connected to one another through shared corners. This layer topology is present in $[C_4H_{12}N_2][Mo_5O_{16}]$ [23].

Charge density calculations: The charge densities of the β-$[Mo_8O_{26}]^{4-}$, $[Mo_3O_{10}]_n^{2n-}$ and $[Mo_8O_{26}]_n^{4n-}$ chains and $[Mo_5O_{16}]_n^{2n-}$ layers are listed in Table 2. They were found to scale with dimensionality: the zero-dimensional β-$[Mo_8O_{26}]^{4-}$ molecular anions have the lowest charge density and the $[Mo_5O_{16}]_n^{2n-}$ layers in $[C_4H_{12}N_2][Mo_5O_{16}]$ exhibiting the highest charge density.

4. Discussion

The profound role of amines in the formation of new inorganic materials is well known [4,5]. Charge density matching between the amine and inorganic component is thought to govern the formation of neutral ammonium–SBU pairs, from which oligomerization and precipitation can occur. The determination of inorganic topology is therefore dependent upon the size, shape and charge of the protonated organic amines.

The work presented here is focused upon the use of four structurally related amines: piperazine, 1,4-dimethylpiperazine, 2,5-dimethylpiperazine and 2,6-dimethylpiperazine. These amines were selected for two reasons. First, they are structurally similar (each containing a piperazine core), they all exist as 2+ cations under the reaction condition employed and they exhibit similar basicities. Second, despite these similarities, these cations have different charge densities, symmetries and hydrogen-bonding properties.

In order to isolate the effects of the amine, a series of reactions was conducted in which the relative mole fractions of each component were fixed: 2.5 MoO_3:1 amine:330 H_2O:2 H_2SO_4. The only difference between reactions was the identity of the amine. When the pH, time, temperature, and relative reactant gel composition between experiments are fixed, direct observation of the effects introduced by the amine structure is possible.

We have observed that several influences are present in the determination of the inorganic structure. First, charge density matching between the protonated amine and inorganic secondary building unit exerts the greatest impact on the inorganic topology. Secondary effects include the symmetry and hydrogen-bonding properties of the amine.

The absence of methyl groups on the $[pipH_2]^{2+}$ cation drastically reduces its volume and surface area with respect to $[1,4\text{-dmpipH}_2]^{2+}$, $[2,5\text{-dmpipH}_2]^{2+}$ and $[2,6\text{-dmpipH}_2]^{2+}$. This decrease in volume results in a subsequent increase in the charge density of the $[pipH_2]^{2+}$ cation. Calculated $[pipH_2]^{2+}$, $[1,4\text{-dmpipH}_2]^{2+}$, $[2,5\text{-dmpipH}_2]^{2+}$ and $[2,6\text{-dmpipH}_2]^{2+}$ volumes, surface areas and charge densities are listed in the Supplementary data. The differences in cation charge density are reflected in the inorganic components. $[C_4H_{12}N_2][Mo_5O_{16}]$, which contains the small $[pipH_2]^{2+}$ cation, contains $[Mo_5O_{16}]_n^{2n-}$ layers. $[C_6H_{16}N_2]_2[Mo_8O_{26}]$ and compounds **1** and **2**, which contain $[2,5\text{-dmpipH}_2]^{2+}$, $[2,6\text{-dmpipH}_2]^{2+}$ and $[1,4\text{-dmpipH}_2]^{2+}$, respectively, include polyoxomolybdates with charge densities that are all significantly lower. See Table 2.

Two important factors should be considered in the analysis of charge density matching. First, the use of van der Waals radii is important for the determination of correct surface area values in low dimensionality anions. The surface of any atom or molecule is often described as being defined by the van der Waals radii of the constituent atoms. For this reason, it is important to use the 'edge' of each anion, as defined by these radii, in the calculation of surface area. Defining a polyhedral representation of an anion using crystallographic coordinates will underestimate the volume and surface area of the structure. This effect is most pronounced in low-dimensionality anions in which a greater proportion of the atoms reside at the edge of the structure. For example, the surface areas of the β-$[Mo_8O_{26}]^{4-}$ anion using the atomic centers and van der Waals radii are 160 and 296 Å^2, respectively (as calculated using the geometrical decomposition method). In addition, the charge densities of the four anions described here were calculated using models constructed from both atomic centers and van der Waals radii and the geometrical decomposition method. The charge densities based upon atomic centers show minimal variation between structures; the β-$[Mo_8O_{26}]^{4-}$, $[Mo_3O_{10}]_n^{2n-}$, $[Mo_8O_{26}]_n^{4n-}$ and $[Mo_5O_{16}]_n^{2n-}$ charge densities are −0.0250, −0.0246, −0.0227 and −0.0249 eÅ^{-2}, respectively. In contrast, the use of van der Waals radii results in charge densities that actually reflect the anion structure, as shown in Table 2. It should be noted that our van der Waals radii correction in the $[Mo_5O_{16}]_n^{2n-}$ layers in $[C_4H_{12}N_2][Mo_5O_{16}]$ affected neither the calculated surface area nor the charge density because the direction of each 'shift' was defined by a vector normal to the central plane of the layer. The shifts in lower-dimensionality anions are based upon central lines in one-dimensional structure or centroids in molecular species. This leads to 'shift' vectors that are not parallel to one another and the calculated surface areas and charge densities are directly affected.

Second, the accessibility of each surface should be considered in calculation of any surface area. The cation–anion interactions in these templated polyoxomolybdates are dominated by hydrogen-bonding interactions that require relatively short N–H···O

distances. Small openings between MoO_6 octahedra and narrow gaps between secondary building units in the structures shown in Fig. 2 represent inaccessible surfaces and should not included in calculated surface areas. The accessibility of all surfaces was evaluated for both methods of calculating surface areas.

In the determination of the molecular surface using the DMS program, we evaluated the role of probe radius on the calculated surface area. Probe radii of 1.4 or 1.5 Å are most commonly used by the structural biology community [10], because these radii represent a water molecule, which is the smallest physically reasonable probe. The effects of varying the probe radius on the calculated surface area of β-$[Mo_8O_{26}]^{4-}$ were investigated for radii between 1.3 and 2.0 Å, see Supplementary data. It was found that deviations across this series were small. A probe radius of 1.5 Å was selected for use in all molecular surface calculations for two reasons. First, this probe radius reflects the increased van der Waals radius of N with respect to O [25], from which all N–H···O hydrogen bonds in these compounds are formed. Second, the sum of the probe radius and the van der Waals radius of O equals the outer limit of most hydrogen-bonding interactions (~3.0 Å).

An inherent assumption in the determination of the molecular surface (as described by Richards [10]) is that the use of a spherical probe is appropriate, and that the probe radius describes the size of the respective probe. However, when the cation–anion interactions include non-spherical organic amines, care needs to be taken in the determination of the surface area. As the probe radius is based upon the length of hydrogen bonds, the molecular surfaces calculated with DMS should represent the maximum possible surface area for a specific anionic structure. Steric effects associated with other parts of the probe molecule can restrict the formation of hydrogen bonds and reduce the accessible surface area. The differences between the surface areas calculated using our geometric decomposition method and the molecular surface determined using the DMS program provide a suitable range of surface areas that reflect both the length of the N–H···O interactions and the non-spherical nature of the organic amines used in this study.

One must be careful not to exclude accessible surfaces in the construction of geometrical decomposition models. For example, four surface area values are listed for the $[Mo_5O_{16}]_n^{2n-}$ layers in $[C_4H_{12}N_2][Mo_5O_{16}]$. See Table 2. The simplest approximation for the surface area, a set of planes shown in Fig. 8c, drastically underestimates the accessible surface area. This is evidenced by the formation of hydrogen bonds between the $[pipH_2]^{2+}$ cations and an oxide ligand that sits below the planes shown in Fig. 8c [23]. Subsequent modifications are shown in Fig. 8a and b. It should be noted that the molecular surface area using DMS is substantially lower, and likely reflects a more appropriate surface area because non-spherical probe effects are minimized in $[C_4H_{12}N_2][Mo_5O_{16}]$ through an approximately perpendicular orientation of the $[pipH_2]^{2+}$ cation to the $[Mo_5O_{16}]_n^{2n-}$ layers.

The ability of amine symmetry to influence the three-dimensional structure in templated materials is known. Examples include the use of chiral organic amines to direct the formation of new noncentrosymmetric molybdates [38,48], sulfated molybdates [49,50], zinc phosphates [51], and gallium phosphates [52]. While none of the four piperazines used in this work are chiral, effects of symmetry can be readily observed.

Despite the structural similarities between amines, distinct differences in inherent symmetries are observed. Piperazine and $[1,4\text{-dmpipH}_2]^{2+}$ contain internal mirror planes and centers of inversion. This is in contrast to $[2,5\text{-dmpipH}_2]^{2+}$ and $[2,6\text{-dmpipH}_2]^{2+}$, which contain only a mirror plane and only an inversion center, respectively. The effects of amine symmetry in $[C_4H_{12}N_2][Mo_5O_{16}]$ cannot be directly observed because the influence of amine charge density is dominant.

The inorganic components in compound **2** and $[C_6H_{16}N_2]_2[Mo_8O_{26}]$, which contain $[1,4\text{-dmpipH}_2]^{2+}$ and $[2,5\text{-dmpipH}_2]^{2+}$, respectively, are constructed from octamolybdate building units. The β-$[Mo_8O_{26}]^{4-}$ molecular anions in $[C_6H_{16}N_2]_2[Mo_8O_{26}]$ are known to be in equilibrium with an α-$[Mo_8O_{26}]^{4-}$ isomer under the reaction conditions employed in this study [53]. This equilibrium has been proposed to occur via a γ-$[Mo_8O_{26}]^{4-}$ intermediate [54], whose structure is present in a host of polyoxomolybate and polyoxofluoromolybdate species including $[Mo_8O_{27}]_n^{6n-}$ chains [55], $[Mo_8O_{26}F_2]^{6-}$ and $[Mo_{16}O_{53}F_2]^{12-}$ molecular anions [56,57] and the $[Mo_8O_{26}]_n^{4n-}$ chains present in compound **2**. This suggests that the molybdate speciation in the $[1,4\text{-dmpipH}_2]^{2+}$ and $[2,5\text{-dmpipH}_2]^{2+}$ reaction is the same. In contrast, the $[Mo_3O_{10}]_n^{2n-}$ chains present in **1** are structurally dissimilar.

The $[2,5\text{-dmpipH}_2]^{2+}$ and $[1,4\text{-dmpipH}_2]^{2+}$ cations in $[C_6H_{16}N_2]_2[Mo_8O_{26}]$ and **2**, respectively, contain internal inversion centers and these compounds crystallize in the monoclinic space group $P2_1/n$ (no. 14). The $[2,6\text{-dmpipH}_2]^{2+}$ cations in **1** do not contain internal inversion centers and they lead to inorganic chains constructed for dissimilar secondary building units. In addition, compound **2** crystallizes in the triclinic space group $P\text{-}1$ (no. 2). The reduction in symmetry of $[2,6\text{-dmpipH}_2]^{2+}$ is manifested in both the structure of the polyoxomolybdate component and the three-dimensional symmetry of the resulting compound.

Another secondary influence over the form of the polyoxomolybdates component in these reactions stems from the formation of extensive hydrogen-bonding networks in such compounds. It has been demonstrated by Brock and others that several principles govern the formation of crystalline solids, including satisfying hydrogen bond donors and acceptors [58,59]. The structure of the polyoxomolybdates component affects the hydrogen bonding network in each compound, as investigated using bond valence sums [60,61] and shown in the Supplementary data. However, the most nucleophilic [38,62,63] oxides are generally either terminal or bound to four or five molybdenum centers, regardless of anion structure [38,64].

In contrast to the polyoxomolybdates components, small structural changes in the amine can greatly affect the hydrogen-bonding preferences. For example, $[1,4\text{-dmpipH}_2]^{2+}$ contains two tertiary amines, while $[2,5\text{-dmpipH}_2]^{2+}$ contains two secondary amines. The relatively flat $[1,4\text{-dmpipH}_2]^{2+}$ cation can lie between neighboring $[Mo_8O_{26}]_n^{4n-}$ chains in **2**, see Fig. 4. Each cation forms a hydrogen bond to each of two adjacent chains, one above and one below. The $[2,5\text{-dmpipH}_2]^{2+}$ cations contain secondary amines, and form four hydrogen bonds per cation. The geometric constraints imposed by the formation of four hydrogen bonds from such a small organic amine promote the existence of molecular β-$[Mo_8O_{26}]^{4-}$ anions over $[Mo_8O_{26}]_n^{4n-}$ chains. While these two anions are constructed from octamolybdate building units, their relative structures are influenced by the hydrogen-bonding networks which stabilize each compound.

5. Conclusion

Isolation of the effects of the amine in the synthesis of new templated molybdates revealed that charge density matching between the protonated organic amines and polyoxomolybdates is the primary influence over the form and composition of the resulting solid under the reaction conditions employed. While amine symmetry and hydrogen-bonding properties can affect the polyoxomolybdates, their influences are secondary.

Supplementary data

Crystallographic data (excluding structure factors) for the structures reported in this paper have been deposited with the Cambridge Crystallographic Data Center as supplementary publication nos. CCDC 713989 and 713990. Tables of bond valence sums for **1** and **2**, a table of Monte Carlo volume integration results, surface areas and charge densities for the organic amines used in this study, a surface area versus probe radius for β-$[Mo_8O_{26}]^{4-}$ and linear fits of surface area versus oligomers size for $[Mo_3O_{10}]_n^{2n-}$, $[Mo_8O_{26}]_n^{4n-}$ and $[Mo_5O_{16}]_n^{2n-}$ are available in the Supplementary data.

Acknowledgments

This is made to Research Corporation and the Howard Hughes Medical Institute for support of the research. A.N.S. gratefully acknowledges support from the National Science Foundation (Award no. CHE-0215963). The authors thank Adam Subhas for performing Gaussian calculations.

Appendix A. Supplementary material

Supplementary data associated with this article can be found in the online version at 10.1016/j.jssc.2009.02.032.

References

[1] R.C. Haushalter, L.A. Mundi, Chem. Mater. 4 (1992) 31–48.
[2] A.K. Cheetham, G. Ferey, T. Loiseau, Angew. Chem. Int. Ed. 38 (1999) 3268–3292.
[3] C.N.R. Rao, S. Natarajan, S. Neeraj, J. Am. Chem. Soc. 122 (2000) 2810–2817.
[4] G. Ferey, J. Fluorine Chem. 72 (1995) 187–193.
[5] G. Ferey, Chem. Mater. 13 (2001) 3084–3098.
[6] C.N.R. Rao, S. Natarajan, A. Choudhury, S. Neeraj, A.A. Ayi, Acc. Chem. Res. 34 (2001) 80–87.
[7] R. Murugavel, M.G. Walawalkar, M. Dan, H.W. Roesky, C.N.R. Rao, Acc. Chem. Res. 37 (2004) 763–774.
[8] S.M. Auerbach, M.H. Ford, P.A. Monson, Curr. Opin. Colloids Interface Sci. 10 (2005) 220–225.
[9] L. Gomez-Hortigueela, F. Cora, C.R.A. Catlow, J. Perez-Pariente, J. Am. Chem. Soc. 126 (2004) 12097–12102.
[10] F.M. Richards, Annu. Rev. Biophys. Bioeng. 6 (1977) 151–176.
[11] A. Monnier, F. Schuth, Q. Huo, D. Kumar, D. Margolese, R.S. Maxwell, G.D. Stucky, M. Krishnamurty, P. Petroff, A. Firouzi, M. Janicke, B.F. Chmelka, Science 261 (1993) 1299–1303.
[12] Q. Huo, D.I. Margolese, U. Ciesla, P. Feng, T.E. Gier, P. Sieger, R. Leon, P.M. Petroff, F. Schueth, G.D. Stucky, Nature 368 (1994) 317–321.
[13] S.H. Tolbert, C.C. Landry, G.D. Stucky, B.F. Chmelka, P. Norby, J.C. Hanson, A. Monnier, Chem. Mater. 13 (2001) 2247–2256.
[14] J. El Haskouri, M. Roca, S. Cabrera, J. Alamo, A. Beltran-Porter, D. Beltran-Porter, M.D. Marcos, P. Amoros, Chem. Mater. 11 (1999) 1446–1454.
[15] P.A. Maggard, P.D. Boyle, Inorg. Chem. 42 (2003) 4250–4252.
[16] S.V. Krivovichev, I.G. Tananaev, B.F. Myasoedov, C. R. Chim. 10 (2007) 897–904.
[17] J. Ling, G.E. Sigmon, P.C. Burns, J. Solid State Chem. 182 (2009) 402–408.
[18] CrysAlis CCD and CrysAlis RED. v. 1.171, Oxford Diffraction Ltd., Abdingdon, UK, 2002.
[19] A. Altomare, G. Cascarano, C. Giacovazzo, A. Guagliardi, J. Appl. Crystallogr. 26 (1993) 343–350.
[20] P.W. Betteridge, J.R. Carruthers, R.I. Cooper, K. Prout, D.J. Watkin, J. Appl. Crystallogr. 36 (2003) 1487.
[21] E. Dowty, ATOMS v. 6.0, Shape Software, TN, USA, 2002.
[22] E.A. Muller, A.N. Sarjeant, A.J. Norquist, Acta Crystallogr. Sect. E 61 (2005) m730–m732.
[23] N. Guillou, G. Ferey, J. Solid State Chem. 147 (1999) 240–246.
[24] C. Huang, DMS. Computer Graphics Lab, University of California San Francisco, CA, USA, 2002.
[25] A. Bondi, J. Phys. Chem. 68 (1964) 441–451.
[26] R.S. Rowland, R. Taylor, J. Phys. Chem. 100 (1996) 7384–7391.
[27] M.J. Frisch, G.W. Trucks, H.B. Schlegel, G.E. Scuseria, M.A. Robb, J.R. Cheeseman, J. Montgomery, J.A.T. Vreven, K.N. Kudin, J.C. Burant, J.M. Millam, S.S. Iyengar, J. Tomasi, V. Barone, B. Mennucci, M. Cossi, G. Scalmani, N. Rega, G.A. Petersson, H. Nakatsuji, M. Hada, M. Ehara, K. Toyota, R. Fukuda, J. Hasegawa, M. Ishida, T. Nakajima, Y. Honda, O. Kitao, H. Nakai, M. Klene, X. Li, J.E. Knox, H.P. Hratchian, J.B. Cross, V. Bakken, C. Adamo, J. Jaramillo, R. Gomperts, R.E. Stratmann, O. Yazyev, A.J. Austin, R. Cammi, C. Pomelli, J.W. Ochterski, P.Y. Ayala, K. Morokuma, G.A. Voth, P. Salvador, J.J. Dannenberg, V.G. Zakrzewski, S. Dapprich, A.D. Daniels, M.C. Strain, O. Farkas, D.K. Malick, A.D. Rabuck, K. Raghavachari, J.B. Foresman, J.V. Ortiz, Q. Cui, A.G. Baboul, S. Clifford, J. Cioslowski, B.B. Stefanov, G. Liu, A. Liashenko, P. Piskorz, I. Komaromi, R.L. Martin, D.J. Fox, T. Keith, M.A. Al-Laham, C.Y. Peng, A. Nanayakkara, M. Challacombe, P.M.W. Gill, B. Johnson, W. Chen, M.W. Wong, C. Gonzalez, J.A. Pople, Gaussian 03, Revision E.01, Gaussian, Inc., Wallingford, CT, 2004.
[28] R.G. Pearson, J. Am. Chem. Soc. 91 (1969) 4947–4955.
[29] R.A. Wheeler, M.H. Whangbo, T. Hughbanks, R. Hoffmann, J.K. Burdett, T.A. Albright, J. Am. Chem. Soc. 108 (1986) 2222–2236.
[30] M. Kunz, I.D. Brown, J. Solid State Chem. 115 (1995) 395–406.
[31] P.S. Halasyamani, Chem. Mater. 16 (2004) 3586–3592.
[32] J.J. Cruywagen, Adv. Inorg. Chem. 49 (2000) 127–182.
[33] P.J. Hagrman, D. Hagrman, J. Zubieta, Angew. Chem. Int. Ed. 38 (1999) 2639–2684.
[34] D.G. Allis, R.S. Rarig, E. Burkholder, J. Zubieta, J. Mol. Struct. 688 (2004) 11–31.
[35] D.J. Chesnut, D. Hagrman, P.J. Zapf, R.P. Hammond, R. LaDuca, R.C. Haushalter, J. Zubieta, Coord. Chem. Rev. 190–192 (1999) 737–769.
[36] I. Lindqvist, Ark. Kemi 2 (1950) 349–355.
[37] W.T.A. Harrison, G.D. Stucky, T.E. Gier, Acta Crystallogr. Sect. C 49 (1993) 1900–1902.
[38] T.R. Veltman, A.K. Stover, A.N. Sarjeant, K.M. Ok, P.S. Halasyamani, A.J. Norquist, Inorg. Chem. 45 (2006) 5529–5537.
[39] J.H. Nelson, A.R. Johnston, A. Narducci Sarjeant, A.J. Norquist, Solid State Sci. 9 (2007) 472–484.
[40] M.I. Khan, Q. Chen, J. Zubieta, Inorg. Chim. Acta 213 (1993) 325–327.
[41] N. Guillou, G. Ferey, J. Solid State Chem. 132 (1997) 224–227.
[42] J.R. Nelson, A. Narducci Sarjeant, A.J. Norquist, Acta Crystallogr. Sect. E 62 (2006) m1448–m1450.
[43] Y. Xu, L.-H. An, L.-L. Koh, Chem. Mater. 8 (1996) 814–818.
[44] S. Chakrabarti, S. Natarajan, Cryst. Growth Des. 2 (2002) 333–335.
[45] R.Q. Fang, X.M. Zhang, H.S. Wu, S.W. Ng, Acta Crystallogr. Sect. E 60 (2004) m359–m361.
[46] K.J. Thorn, A. Narducci Sarjeant, A.J. Norquist, Acta Crystallogr. Sect. E 61 (2005) m1665–m1667.
[47] J.R. Nelson, A. Narducci Sarjeant, A.J. Norquist, Acta Crystallogr. Sect. E 62 (2006) m1731–m1733.
[48] M. Inoue, T. Yamase, Bull. Chem. Soc. Jpn. 68 (1995) 3055–3063.
[49] E.A. Muller, R.J. Cannon, A.N. Sarjeant, K.M. Ok, P.S. Halasyamani, A.J. Norquist, Cryst. Growth Des. 5 (2005) 1913–1917.
[50] J.R. Gutnick, E.A. Muller, A.N. Sarjeant, A.J. Norquist, Inorg. Chem. 43 (2004) 6528–6530.
[51] T.M. Nenoff, S.G. Thoma, P. Provencio, R.S. Maxwell, Chem. Mater. 10 (1998) 3077–3080.
[52] H.-M. Lin, K.-H. Lii, Inorg. Chem. 37 (1998) 4220–4222.
[53] W.G. Klemperer, W. Shum, J. Am. Chem. Soc. 98 (1976) 8291–8293.
[54] M.L. Niven, J.J. Cruywagen, J.B.B. Heyns, J. Chem. Soc. Dalton Trans. (1991) 2007–2011.
[55] I. Boeschen, B. Buss, B. Krebs, Acta Crystallogr. Sect. B 30 (1974) 48–56.
[56] B. Kamenar, B. Kaitner, N. Strukan, Acta Crystallogr. Sect. C 46 (1990) 2249–2251.
[57] A.K. Stover, J.R. Gutnick, A.N. Sarjeant, A.J. Norquist, Inorg. Chem. 46 (2007) 4389–4391.
[58] C.P. Brock, J.D. Dunitz, Chem. Mater. 6 (1994) 1118–1127.
[59] M.C. Etter, J. Phys. Chem. 95 (1991) 4601–4610.
[60] I.D. Brown, D. Altermatt, Acta Crystallogr. Sect. B 41 (1985) 244–247.
[61] N.E. Brese, M. O'Keeffe, Acta Crystallogr. Sect. B 47 (1991) 192–197.
[62] K.R. Heier, A.J. Norquist, C.G. Wilson, C.L. Stern, K.R. Poeppelmeier, Inorg. Chem. 37 (1998) 76–80.
[63] A.J. Norquist, M.B. Doran, D. O'Hare, Inorg. Chem. 44 (2005) 3837–3843.
[64] D.J. Hubbard, A.R. Johnston, H. Sanchez Casalongue, A.N. Sarjeant, A.J. Norquist, Inorg. Chem. 47 (2008) 8518–8525.